ISSN: 2230-9926

*Available online at http://www.journalijdr.com*

IJDR

*International Journal of Development Research*
*Vol. 10, Issue, 06, pp. 36407-36416, June, 2020*
https://doi.org/10.37118/ijdr.18951.06.2020

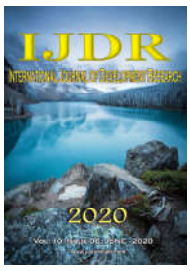

RESEARCH ARTICLE OPEN ACCESS

# WELDMENTS WITH FILLET JOINTS SUBMITTED TO "IN-PLANE" QUASI-STATIC AND IMPACT TORSION LOADS

***Anderson Dal Molin and Ivan Guerra Machado**

Federal University of Rio Grande do Sul (UFRGS), PPGE3M, Welding & Related Techniques Laboratory (W&RTL), Porto Alegre, Rio Grande do Sul, Brazil

**ARTICLE INFO**

***Article History:***
Received 17th March, 2020
Received in revised form
26th April, 2020
Accepted 04th May, 2020
Published online 25th June, 2020

***Key Words:***
Welding,
Structural Ductility,
"In-plane" quasi-static and impact torsional loads.

****Corresponding author:***
***Anderson Dal Molin***

**ABSTRACT**

This paper presents partial results of a broader research in progress involving fillet joints welded with Gas Metal Arc Welding and using consumables that produce weld metals with a large difference in ultimate tensile stress and ductility (classes AWS ER70S-6 e AWS ER120S-G). Therefore, two kinds of weldments were made with one of the members in "balance" and keeping welds with their original finish. One weldment was made with two weld beads transverse to the loading direction ("WT") and the other with welds in a C shape, having beyond those two weld beads, another parallel to the loading direction, connecting them. Only those weldments made with AWS ER120S-G were loaded with and without preheating. Then, all weldments were submitted to "in-plane" quasi-static and structural impact torsional loads. Among the main results, the influence of the 150 °C preheating on the weldment with AWS ER120S-G electrode is highlighted, for apparently it also made the weldment more ("structurally") ductile. With quasi-static loads and considering the "C" weld configuration, this preheating reduced around 13% the joint hardness and increased around 11% the weldment strength, when compared to other manufactured at room temperature. Preheating also increased around 7% the weldment strength to impact loading.



**Citation:** ***Anderson Dal Molin and Ivan Guerra Machado.*** "Weldments with fillet joints submitted to "in-plane" quasi-static and impact torsion loads", *International Journal of Development Research*, 10, (06), 36407-36416.

## INTRODUCTION

The lack of planning in the use of steel as a structural material can generate problems, which could be avoided in the conception and design phase. Several pathologies would not occur if the connections between the elements were carefully detailed and performed. Also, structures with high susceptibility to instability and torsion phenomena can be formed because of the combination of aesthetic requirements of projects and the trend to reduce weight to minimize aggregate costs. Despite the apparent simplicity of welded joints, computational modeling shows that the internal stress systems where there is load transference between members are extremely complex which is reported by Machado (2011), where was discussed that structural integrity is not only dependent on the individual mechanical properties of the members that make up the structure but is a consequence of several other factors, including the type of loading and the state of the stresses. However, in this critical review, he discussed the analytical design of fillet welded joints under the concepts of local elasticity and plasticity theory. The comparison between the analytical methods presented and an experimental analysis would make it possible to detail the design of welded joints. Based on this context and the absence of specific bibliography related to this subject, this research was proposed. The work was aimed at determining the influence of torsional loads, in the plane, quasi-static and dynamic with structural impact on weldments with fillet joints, using consumables that deposit weld metals with high difference in tensile strength and ductility resistance. It is highlighted that the weldments were tested and the original manufacturing finishing was fully kept. The analysis of a structure under impact requires knowledge of the material's mechanical behavior. In fact, Dieter (1981) highlights that it is necessary to describe the material response when subjected to this type of loading.

That is, the impact on structures is a phenomenon that comprises a wide range of non-trivial concepts, such as non-linearities, inertia effects, contact, effects of material deformation rate, buckling, and propagation of elastic and plastic waves. Cleavage fracture is the most fragile form of fracture that can manifest in steels. Broek (1984), for example, shows that the probability of its existence increases at lower temperatures and higher deformation rates, thus occurring a transition, known in steel as ductile-fragile, but below this transition, lower energy is required to steel's fracture and that it behaves in a fragile manner. The fracture process involves formation and propagation of cracks, the fracture mode being dependent on the propagation mechanism. The ductile fracture is characterized by an extensive plastic deformation in the vicinity of an advancing crack. In addition, the process proceeds relatively slowly as the crack length increases. This type of crack is called stable. In the case of a fragile fracture, cracks can spread extremely quickly, accompanied by little plastic deformation. Such cracks are called unstable, and the crack propagation, once started, will continue spontaneously without increasing the magnitude of the applied stress (Callister 2009). According to Alves (2005), the classic fracture mechanics quantifies the growth, speed and dissipation energy of crack propagation in terms of Euclidean geometry. However, it is known that cracks are fractal objects and, therefore, the physical properties of their propagation can be treated in an explicit way by clarifying the fractal properties of their surface (Dauskardt *et al*., 1990). Therefore, it is possible to relate the morphology of a fracture surface to the conditions of the fracture process such as: material, loading, temperature, environment, direction and crack growth rate. When a body is sought by a slow loading caused by an external force, this body responds with all inertia it possibly has, as there is enough time for the entire structure to "relax". Yet, Meyers, (1994) states high loading rates (dF/dt) turn this event into a localized phenomenon, changing from section to section of the body, which causes stresses concentration and deformation. Therefore, it seems that a part of the body cannot "feel" the request. However, his model compares only a simple material but in this research are tested a welded union using consumables that produce weld metals with a large difference in ultimate tensile stress.

Deformation-sensitive materials can vary in their mechanical properties as changes in strain rates are imposed. In impact situations where the presence of high strain rates is verified, it is appropriate to investigate the mechanical behavior of the material in the referred conditions through dynamic tensile tests with the adjustment of the strain rate. The response of a given structure subjected to the action of dynamic loading (impact) depends on the speed of impact and the rate of deformation imposed. For materials sensitive to the strain rate, there are changes in the mechanical properties according to the increase in the strain rate (Jones, 2012). The deformation of a material consists in elastic and plastic phases, being these two phases relatively easily identified in the stress-strain curves. For structural engineering applications, according to Neal (1956), this curve is often idealized and represented in a simplified way, without considering the steel hardening effect. However, in this study it is evaluated a structural material and depending the thermo mechanical treatment to which it was submitted, or the union formed by dissimilar materials, the stress-strain curve can take on very different forms.
However, the mechanical properties of a material are usually obtained through tensile tests performed under static conditions, that is, with low strain rates. According to Dieter (1981) the deformation rates for static condition vary from $10^{-4}$ to 100 $s^{-1}$ and in Meyers (1994) the static condition is achieved with deformation rates between $10^{-5}$ to 101 $s^{-1}$. Various codes, standards, and recommendations, among others, can be used for dimensioning welded joints. All of them are based on simplifications, which many times may be summarized in finding the forces acting orthogonally on the plane determined by the weld bead throat, with their respective stresses in this plane (assumed to be constant). Then, the forces are combined to satisfy some specific criteria.

When groups of welds are loaded in shear by an external load that doesn't act through the center of gravity of the group, the load is eccentric and will tend to cause relative rotation and translation between the parts connected by welds. The point over which the rotation tends to happen is called the instantaneous center of rotation, Blodgett (1966) assign that its location depends on the load eccentricity, weld group geometry and weld deformation at different angles of the resulting force relative to the weld axis. But in this reference book, the effect of the deformation rate is not considered, that is, it is only considered static loads. Cantilever "beams" with loading outside the center of gravity, such as the situation of this experiment, can have the magnitude calculated by the association between the primary shear stress ($\tau'$) obtained by Equation 1 and the secondary shear stress or "twist" ($\tau''$) of the welds, produced by the moment in the support, as presented in Equation 2.

$$\tau' = V/A \quad (1)$$

where (V) is the shear force reaction and (A) is the sheared area determined by the weld throat (all welds).

$$\tau'' = (M.r)/J \quad (2)$$

where "M" is the moment caused by loading, "r" is the distance from the centroid of the weld group to the point of weld of interest, and "J" is the second polar moment in the area of the weld group. The primary and secondary shear can be determined when weld bead sizes are known, and their results combined as vectors provide a good approximation of the maximum shear stress caused by loading. Adopting the weld width with unit values allows each fillet weld to be treated as a line and "J" becomes the second polar unit moment of area "$J_u$", which has the same value regardless of the size of the weld bead, considering that the values of the weld bead legs size are the same. For fillet welds with equal legs (isosceles right triangle), the relationship between "J" and the unit value is obtained by Equation 3.

$$J = \sqrt{2}/2.z.Ju \quad (3)$$

where "z" is the bead leg size and "$J_u$" can be found by conventional methods for an area with unit width. The throat areas and the second polar unit moments of area for weldments with fillet joints are commonly found in tables and standards.

## MATERIAL AND METHODS

Normalized ASTM A-36 and EN S235 JR steels, both in the form of plates with thicknesses of 25.4 mm and 76.2 mm, respectively, were selected due to their wide use in the most diverse types of metallic structures. Chemical analyses of these

steels were performed by optical emission spectrometry and their chemical compositions are presented in Table 1(a) in weight percent (wt. %); values meet the respective standards (ASTM A36/A36M-14, 2014 and EN 10025-2: 2004). Mechanical properties required for these steels by the respective standards are presented in Table 1(b). AWS ER70S-6 and AWS ER120S-G were the electrodes used, both solid wires with 1.2 mm diameter. Chemical analysis of the relevant elements is shown in weight percent (wt. %) in Table 2(a), while mechanical properties are shown in Table 2(b), following the quality certificate provided by the manufacturer ESAB (2019) and meeting the requirements AWS (2006). The choice of consumables with such a big difference in mechanical properties is to fulfill one of the objectives of this study, which is to investigate the effect of mechanical resistance and ductility on the mechanical behavior of welded joints. Therefore, according to AISC (2006) the AWS ER70S-6 is defined as "matching" because it has similar mechanical resistance to the base metals, while the AWS ER120S-G is considered "overmatching" because its mechanical resistance is much higher than that of base metals. Welds were produced by Gas Metal Arc Welding (GMAW), or electric arc process with gas protection and consumable electrode, in flat position using a system composed by a TransPuls Synergic 4000R Fronius power source and an MA1400 Yaskawa Motoman Robotics robot. In all cases, it was used: direct current electrode positive polarity (DCEP); a mixture of 85% Ar and 15% $CO_2$ as shielding gas; 15 L/min flow rate; neutral angles of work and displacement, and contact-tip-to-work distance (CTWD) equal to 18 mm. Additional information is shown in Table 3.

Fig. 1 shows details of two types of weldments used in this study and positions of weld beads with 7 mm legs. The so-called "transversal to the loading direction" (indicated with "T") has weld beads positioned transversely to the direction of the load application ("F" in Fig. 1). Another weld bead in the direction of the load application, indicated with "L", exists in weldments called "in C" (weld beads form a "C") in addition to the two transverse weld beads like the previous ones. The member whose thickness is 76.2 mm in the EN S235 JR steel is cantilevered and supports the side-impact, which is made directly on a "hit plate" (dimension 30×60 mm) fixed on its side. Preliminary tests have indicated this arrangement makes the deformation of the cantilevered member and its support imperceptible. However, the efficiency of the impact transfer to the weld beads was not measured. Weldments were manufactured with conditions identical to those shown in Table 3 to measure the legs of the weld beads and the hardness. A typical weld bead macrograph is shown in Fig. 2, from which leg size was measured and microhardness tests (Vickers) were performed with a load of 0.5 kgf applied according to ASTM standard ASTM E384 (2017).

The device for performing quasi-static tests was developed at W&RTL. It is specifically an arrangement of individual components, connected, suitable to produce torsion in the cantilevered element of the welded assembly, which allows the load to be applied linearly by a hydraulic piston in an almost static manner. The load produces torsion that is transferred to the weldment, and the load reading is carried out through a load cell. The basic structure of this hydromechanical system consists of a hydraulic device connected to a piston, machine structure (fixed gantry), control items (load cell, strain gauges, data acquisition system), and other items (for supporting specimen and measuring devices). The load cell model Q-10T, which makes up the device, is based on the theory of extensometry by a complete Wheatstone bridge, and the load cell deformation data are acquired by the universal digital multichannel system Spider 8 - HBM. Each quasi-static test was performed once, as in any case an abnormal situation was identified. A device was also developed at W&RTL for performing dynamic tests of torsional impact "in-plane", which allows the application of loading through an impact hammer. This system is like a Charpy impact test only in terms of the principle of operation, as this is a structural impact system. The device for the test is shown in Fig. 3(a) and was designed to meet the theoretical concepts presented for example in Beléndez (2007). The weldment is positioned for the test (Figure 3(b)), having been fixed and receiving the impact to transmit the torsion to the weld beads. The "lever arm" up to the hammer is approximately 1.7 m, with the cylindrical keel reaching (in a "line") the hit plate fixed on the side of the beam in balance (in its thickness).

**With reference to Figure 3, it can be seen in:**

- the developed device prepared in the test launch position at 110°.
- the specimen positioned and the structural impact hammer at the exact point of impact in order to transmit torsion to the weld beads.
- the highlight for the reader of the detail being presented in (d), (e) and (f).
- the region of the puncture just before the impact.
- exactly when the punch reaches the sacrifice plate, the linear velocity vector (*vx*) used to calculate the impact energy was inserted.
- the puncture moments after the impact, where the separation of the parts occurs.

The horizontal component of the pendulum velocity at the moment of impact and immediately after it was determined using two experimental methods (see below), with two specimens tested in each case. The moment immediately after impact was considered as being the moment of the separation between the cylindrical impact keel and the cantilevered member of the weldment. So, after getting the horizontal component of the pendulum velocity, force and kinetic energy on impact were also analytically calculated using Beer and Johnston (2013). In the first experimental method, a photoelectric sensor was used. In this device, the signal is interrupted by the passage of two pre-defined fixed elements in the hammer at impact moment. In the second experimental method, a high-speed camera (Phantom, model V411) was used, with a NIKKOR 105 mm/f2.8 lens manufactured by Nikon and a UV filter. The images were acquired with 7000 frames per second and a resolution of 512 × 512 pixels, which were processed by the dedicated Phantom Camera Control (PCC) software. Events that occur in intervals as small as 0.01 s can be easily visualized due to the very high rate of image acquisition. The hammer was filmed immediately before and after impact, with the software even enabling the cartesian decomposition of the velocity vector by analyzing the captured images. It allowed obtaining the horizontal impact velocity, which was considered in this work. For measurements correlating the hammer's release angles with the impact velocities, the hammer was released at every 15° of elevation up to 90° and, afterward, from 110° and 120° with three releases at each angle. However, the experiments were carried

out every 5°, between 50° and 80°, to verify when the fracture started at the welded joint. The kinetic energy "$E_c$" (J) at impact was calculated by Equation 4.

$$E_c = m.v_1^2/2 \quad (4)$$

where "m" is the impact mass (mass of the hammer, equal to 252 kg) and "$v_1$" is the horizontal velocity of the pendulum (m/s) at the impact moment. The effective or average force "F" (N) of impact can be obtained through Newton's second principle. It states that "the rate of change in the amount of movement of a material point is proportional to the applied force and occurs in the direction where this force works". Consequently, the impulse of a force is given by the product of this force by the time it acts (more precisely the time integral of the force), which is equal to the product of the mass that moves by the difference in its velocities before and after the impact, regardless this impact is elastic or inelastic. Therefore, this force was estimated by Equation 5.

$$F = m.(v_1 - v_2)/\Delta t \quad (5)$$

where "$v_2$" the horizontal velocity of the pendulum (m/s) immediately after impact and "$\Delta t$" is the time interval (s) of occurrence of this event. Table 4 shows the average results of three releases (with some exceptions, see notes) for different release angles, horizontal impact velocities, and the corresponding estimated kinetic energies (Equation 4) for the hammer with a mass of 252 kg.

In a cross-section of a welded bead, the dilution can be calculated using the ratio between base metal melted area and the whole weld metal area. For carbon and low alloy steels, in general, dilution has little effect on weld metal strength. However, in high strength steels, this factor may be relevant in the performance of the welded joint. The following dilutions were measured for each weldment: (a) A70TA: 36,8 %; (b) A120TA: 39,0 %; (c) A120T150: 42,7 %. It can be seen that the maximum difference is less than 6% and here it is considered to be negligible.

## RESULTS AND DISCUSSION

Regions of welded joints with their respective hardness are presented in Fig. 4 (see Table 3 for the weldments codes). The hardness values of the heat affected zone (HAZ) are very close to the weldments made at room temperature with AWS ER70S-6 (A70TA) and AWS ER120S-G (A120TA) consumables due to the identical welding parameters used in this work. Otherwise, the hardness values are smaller for the A120T150, as the base metal was preheated to 150°C. However, weld metal (WM) of the A70TA weldment shows hardness around 120 HV0.5, lower than that of the A120T150 and approximately 150 HV0.5 lower than the A120TA. When the A120TA weldment is compared with the A120T150, the maximum hardness values of WM and HAZ were reduced by approximately 45 HV0.5 and 60 HV0.5, respectively.

Figure 4. Hardness in welded joints (HAZ: heat affected zone; BM: base metal; WM: weld metal). Figs. 5 and 6 show results of quasi-static tests for weldments with transversal weld and "C" weld beads, respectively. At least two groups of relevant information can be extracted from these tests, which are summarized in Table 5. The first group associated with the maximum loads resisted immediately before the sudden reduction of their values due to the beginning of fracture in the joint. In the second group, there is an indicative directly associated with the structural ductility of the weldments. As conceptually defined by Machado (2013), it is the area under each curve shown in Figs. 5 and 6, whose unit is the same as the impulse (kN.s). Therefore, this area means the multiplication of the period by the active load that a weldment supports until the fracture starts. Evidently, this fact does not guarantee the complete structural continuity of the weldment and does not attest to the capacity of fulfilling its function.

Therefore, considering those two groups of information, the following synthesis can be provided:

- Preheating had a great effect on weldment using AWS ER120S-G electrode. It reduced the hardness of the welded joint when compared to that welded at room temperature. Apparently, this preheating made the weldment structurally more ductile, since the A120T150 started to support approximately 11% more load than the A120TA, for both weld configurations (transverse and "C") and without a fracture occurrence.
- Proportionality between the areas is seen after analyzing the curves in the quasi-static tests. The weldment with the A120T150 electrode presented approximately 50% more area when compared to the A120TA. The A120TA presented approximately 18% more area than the A70TA, regardless of the configuration of weld beads used (transverse or "C").
- Electrodes used in weldments A120TA and A120T150 are the same, but due to preheating the hardness of weld metal A120T150 is around 13% lower than A120TA. However, for both transverse and "C" weld beads, there is a notable difference between the areas under the curves in the quasi-static test. For the A120TA, the area is approximately 50% smaller than that of A120T150.

The energies that the hammer must develop for the impact to start fracturing the welded joint are shown in Table 6, with the hammer released at 5° elevation intervals. Therefore, the exact magnitude of the energy required to initiate the fracture on impact may be slightly less than that shown. The increase in ductility produced by preheating is clear since the weldment A120T150 is the one that supports the largest (structural) impact and is the most resistant in the quasi-static test. Results obtained for quasi-static and structural impact tests (angle of hammer elevation of 110°) are presented in Table 7, which also shows the analytical value of the maximum resisted load, using Equations 1 and 2, and the size of the weld bead leg (z = 7 mm). A complete separation between members of the weldments has occurred. The elevation angle of the impact hammer of 110° was used because it is the highest elevation where the operation is safe and because it ensures the highest speed at the impact moment, as shown in Table 4.

**Regarding the data presented in Table 7, it is worth mentioning:**

- As adopted by most standards or Codes (there are exceptions), mechanical properties are related to those specified for the consumable, according to Table 2(b), and not to the weld metal produced by it at the joint under consideration. This is attributed to the dimensioning of the welded joint, which is based on the

**Table 1(a). Chemical compositions of ASTM A-36 and EN S235 JR steels**

| Base Metal | Chemical elements (wt. %) | | | | | |
|---|---|---|---|---|---|---|
| | C | Si | Mn | P | S | Cu |
| ASTM A-36 | 0.161 | 0.189 | 0.785 | 0.027 | 0.011 | 0.005 |
| EN S235 JR | 0.209 | 0.227 | 1.107 | 0.021 | 0.013 | 0.0098 |

**Table 1(b) - Mechanical properties specified for ASTM A-36 and EN S235 JR steels**

| Base Metal | Tensile Strength (MPa) | Yield Point (MPa) | Minimum Elongation (%) |
|---|---|---|---|
| ASTM A-36 | 400 – 550 | 250[(a)] | 20[(a)] |
| EN S235 JR | 360 – 510 | 215[(a)] | 24[(a)] |
| Notes: (a) for shapes | | | |

**Table 2(a). Chemical compositions of consumables (ESAB, 2019)**

| Electrode | Chemical elements (wt. %) | | | | | | | |
|---|---|---|---|---|---|---|---|---|
| | C | Si | Mn | P | S | Cr | Ni | Mo |
| AWSER120S-G | 0.10 | 0.68 | 1.77 | 0.015 | 0.010 | 0.36 | 1.84 | 0.45 |
| AWS ER70S-6 | 0.083 | 0.87 | 1.45 | 0.010 | 0.015 | 0.01 | 0.01 | 0.04 |

**Table 2(b). Mechanical properties of consumables (ESAB, 2019)**

| Electrode | Tensile Strength (MPa) | Yield Point (MPa) | Elongation (%) | Energy Absorbed on Charpy-V Impact at Temperature |
|---|---|---|---|---|
| AWS ER120S-G | 900 | 850 | 18 | 55 J @ -40°C |
| AWS ER70S-6 | 480 | 400 | 22 | 27 J @ -30°C |

**Table 3. Welding conditions**

| Electrode (Weldment code) | Preheating Temperature (°C) | Average Voltage (V) | Average Current (A) | Welding Speed (mm/s) | Average Welding Energy (kJ/mm) | Wire Feed Speed (m/min) |
|---|---|---|---|---|---|---|
| Aws er70s-6 (a70ta) | Room | 26.5 | 242 (± 3) | 7.0 | 0.91 (+0.02/-0.01) | 6.5 |
| Aws er120s-g (a120ta) | Room | | | | | |
| Aws er120s-g (a120t150) | 150 | | | | | |

**Table 4 - Velocity and average hammer impact energies for different elevation angles**

| | Hammer release angle (°) | | | | | | | | | | |
|---|---|---|---|---|---|---|---|---|---|---|---|
| | 15 | 30 | 45 | 60 | 70[(a)] | 75 | 80[(a)] | 85[(a)] | 90 | 105 | 110[(b)] |
| Impact velocity (m/s) | 1.28 | 2.49 | 3.71 | 4.84 | 5.53 | 5.83 | 6.21 | 6.49 | 6.77 | 7.59 | 8.17 |
| Impact energy (kJ) | 0.21[(c)] | 0.78[(c)] | 1.73 (+/- 0.01) | 2.95 (+/- 0.01) | 3.85 | 4.28 (+/- 0.06) | 4.86 | 5.31 | 5.77 (+/- 0.03) | 7.28 (+/- 0.04) | 8.41 (+/- 0.12) |

Notes: (a) deviation from the mean not available; (b) average of 6 hammer releases; (c) deviation from the mean less than 0.01 kJ.

**Table 5 - Maximum resisted loads and areas under the curves in the tests presented in Figures 5 and 6**

| Weldment code | Maximum Hardness in Weld Metal (HV0.5) | Maximum resisted load (kN) | | Area under the curve (kN.s) (*) | |
|---|---|---|---|---|---|
| | | Transverse weld beads | Weld beads in "C" | Transverse weld beads | Weld beads in "C" |
| A70 TA | 261 | 68 | 83 | 1181 | 1743 |
| A120 TA | 406 | 86 | 104 | 1377 | 2174 |
| A120 T150 | 354 | 95 | 116 | 2104 | 3189 |

**Table 6. Energies needed to start fracture at the welded joint in the impact tests**

| Weldment code | Type | Maximum hardness in WM (HV0.5) | Release angle (°) | Impact energy (kJ) |
|---|---|---|---|---|
| Transverse weld beads | A70TA | 261 | 50 | 2.05 |
| | A120TA | 406 | 55 | 2.47 |
| | A120T150 | 354 | 60 | 2.95 |
| Weld beads in "C" | A70TA | 261 | 55 | 2.45 |
| | A120TA | 406 | 65 | 3.34 |
| | A120T150 | 354 | 70 | 3.85 |

**Table 7. Impact forces and energies for the complete separation of welded members (*)**

| Weldment code | Transverse weld beads | | | | | Weld beads in "C" | | | | |
|---|---|---|---|---|---|---|---|---|---|---|
| | Maximum resisted load (kN) | | | Energy (kJ) | | Maximum resisted load (kN) | | | Energy (kJ) | |
| | Analytics (**) | Quase-static | Impact | In the Impact | After the impact | Analytics (**) | Quase-static | Impact | In the Impact | After the impact |
| A70TA | 43 | 68 | 54 | 8.29 | 4.18 | 49 | 83 | 73 | 8.53 | 3.16 |
| A120TA | 84 | 86 | 65 | 8.35 | 3.62 | 103 | 104 | 90 | 8.51 | 2.13 |
| A120T150 | 84 | 95 | 69 | 8.37 | 3.55 | 103 | 116 | 98 | 8.43 | 1.66 |

Note: (*) hammer elevation angle of 110°; (**) considering welds as a line and consumables yield limits.

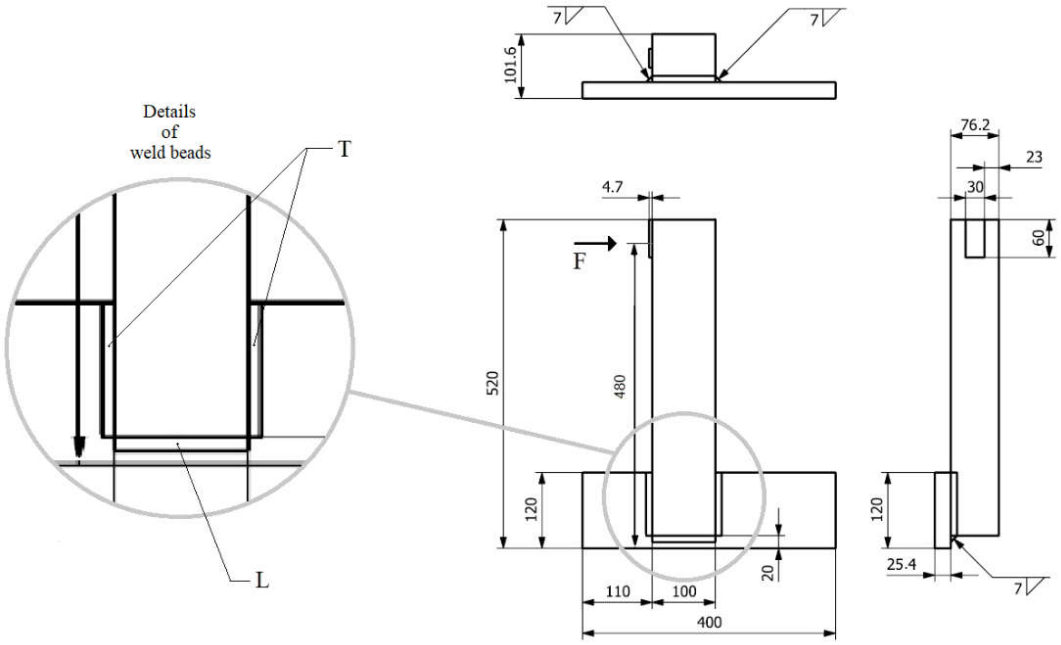


**Figure 1. Weldments with beads "transversal to the load" (indicated with "T") and in "C", which additionally has a weld bead in the direction of loading (indicated with "L")**

**Figure 2. Macrograph of welded joint A120T150 (Nital 10% reagent)**

nimum (nominal) values specified for the class of the consumable, even if the results of the mechanical tests carried out on specimens standardized by these norms or codes are higher.

- When analyzing the weldment made with the A70TA electrode, the model used for the analytical calculation of the maximum resisted load underestimates the resistance of the welded joint since the maximum resisted load in the quasi-static test is approximately 58% higher. When analyzing the weldments A120TA and A120T150, it is observed an increase in the resistance of the beads by only 2% and 11%, respectively, related to the analytical model. This difference can be attributed to the fact that the AWS ER 120S-G electrode has a mechanical strength much higher than the base metals used (Tables 1(b) and 2(b)) and to occurrence of base metal removal in some points of the welded joint.

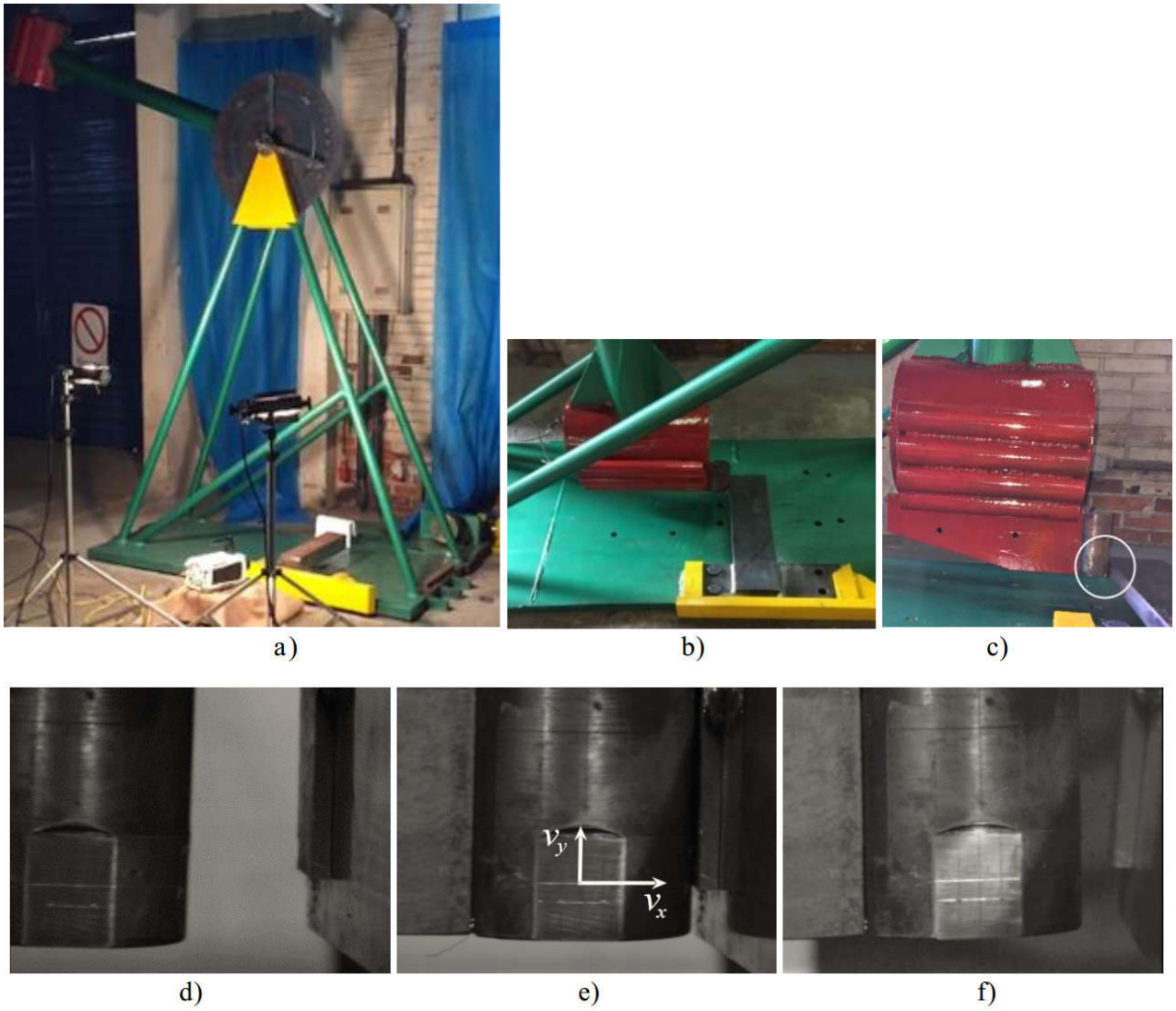


**Figure 3. Images of the impact device developed at W&RTL as well as cylindrical keel details (see text)**

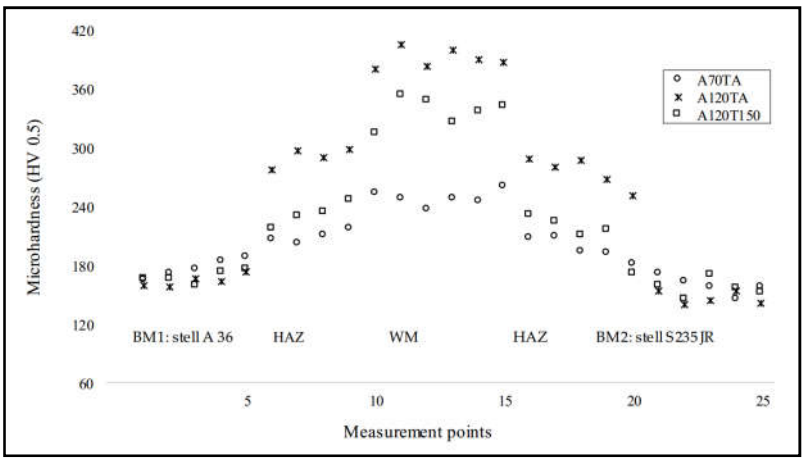


**Figure 4. Hardness in welded joints (HAZ: heat affected zone; BM: base metal; WM: weld metal)**

- When comparing the maximum resisted loads in quasi-static and impact tests, the weldments resist lower impact loads. For configuration of transverse welds, the A70TA, A120TA and A120T150 weldments resist, respectively, impact loads of 26%, 32% and 38% lower than quasi-static loads.
- Preheating also influenced the resistance to impact loading. When analyzing the "C" configuration, weldments A120T150 and A120TA were welded with the same electrode but different preheating. This resulted in weldment A120T150 to be around 8% stronger than A120TA.

Figure 7 (a) shows a fracture on welded assembly A120TA due to impact loading transverse to weld beads, highlighting the approximate location of the chosen point to perform analysis of the fractured surface. Figures 7 (b - d) show images

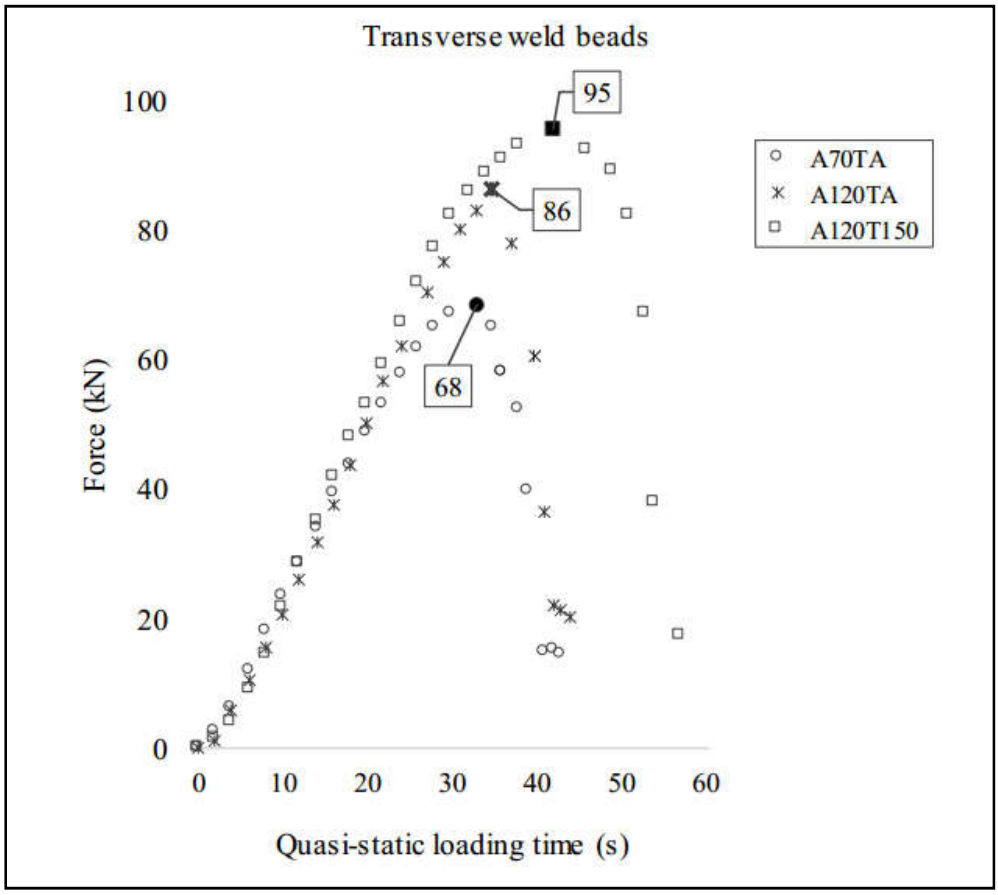


**Figure 5. Quasi-static loading time and resistance of transverse weld beads**

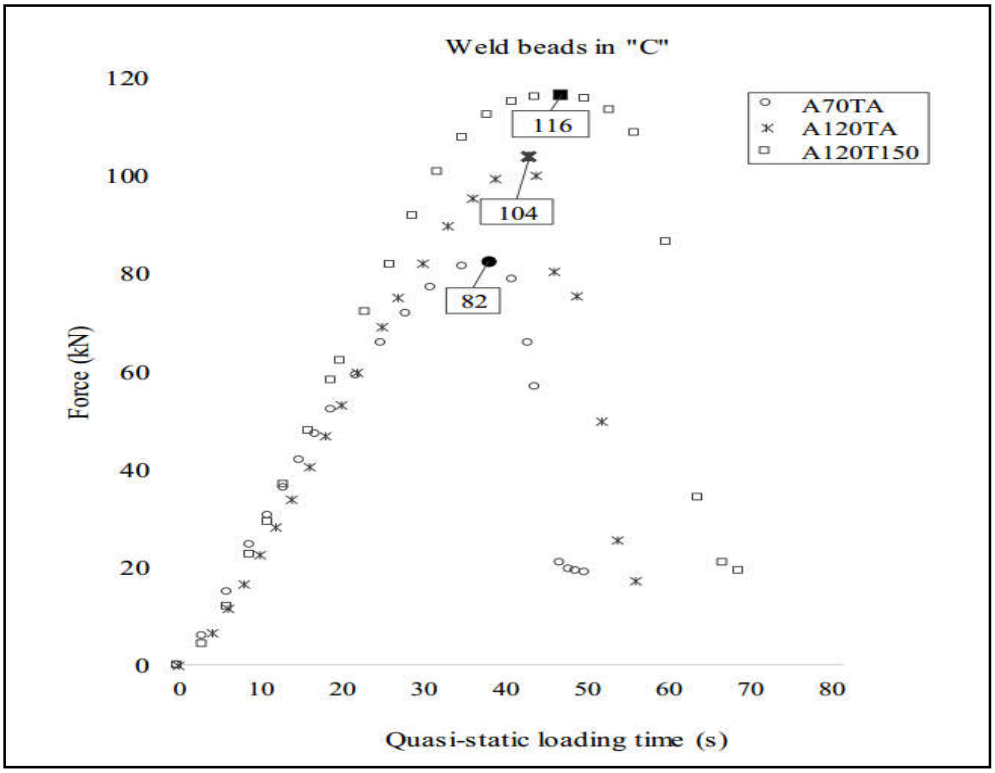


**Figure 6. Quasi-static loading time and resistance of the weld beads in "C"**

of the fracture surface of the weld metal of the different configurations used in this research (indicated in the legend), subjected to impact loads transversal to the weld beads, obtained by scanning electron microscopy (SEM), with the purpose of analyzing the evolution of micro fracture mechanisms.

The following observations can be made from the analysis of the morphology of the images in Figure 7:

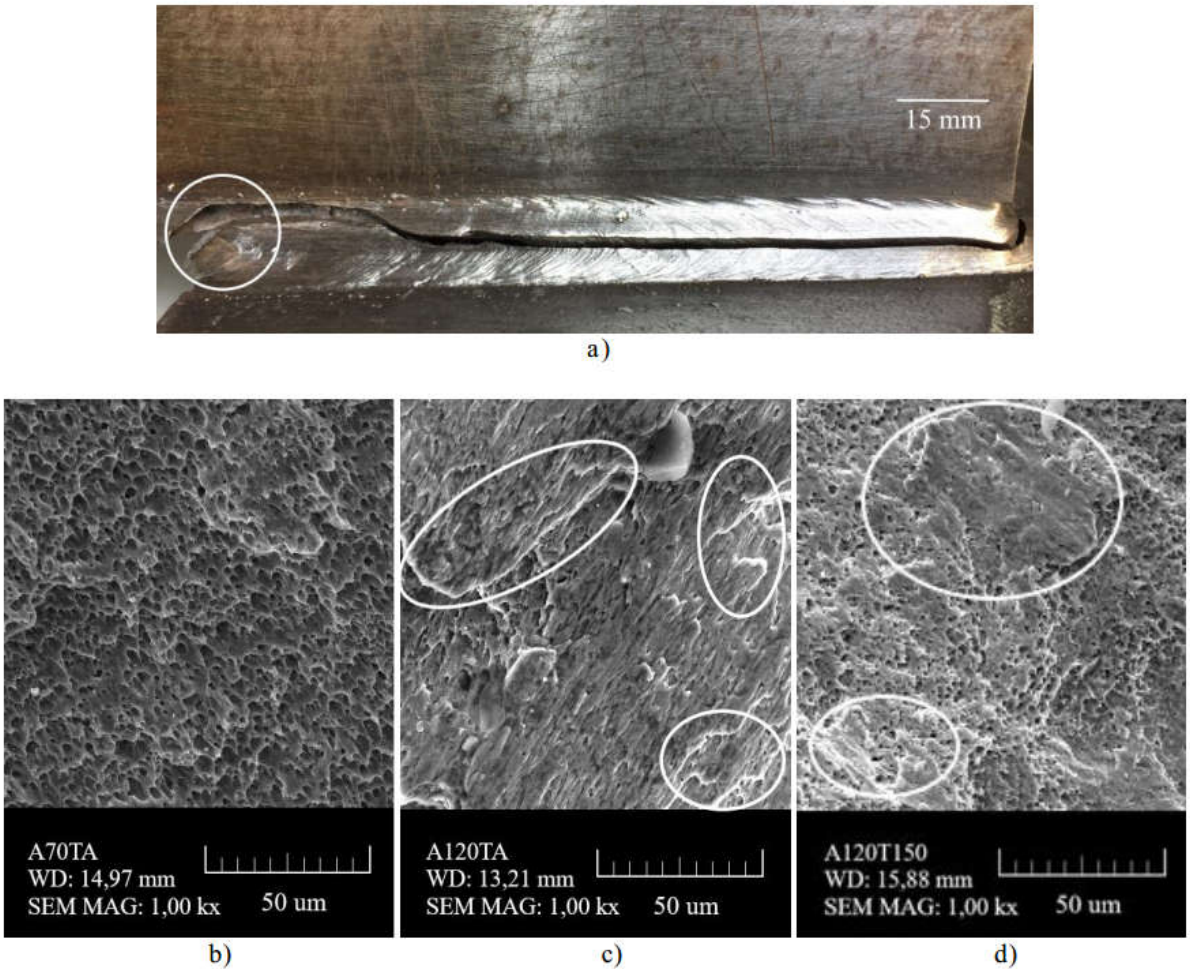


**Figure 7. (a) Fractured weldment (A120TA) lateral view; (b-d) Fractures surfaces of different weldments (SEM - see text)**

- Figure 7 (b) shows the A70TA weldment weld metal fractured surface. It can be seen a large presence of spherical micro cavities (dimples) and extensive plastic deformation, with shear produced by impact (the micro-voids produced by coalescence are inclined). So it is a ductile type fracture.
- Figure 7 (c) shows the A120TA weldment weld metal fractured surface. There is a fragile fractured region with facets and cleavage lines (highlighted) and flat regions, being notice intragranular fractures in a regular region (with low degree of plastic deformation).
- Figure 7 (d) shows the A120T150 weldment weld metal fractured surface. The presence of a fibrous and shear zone is noticed. The microscopic aspect is characterized by rupture of connections and cleavage is present on a very small scale and on not well defined planes, as highlighted in the image, which is characteristic of semi-fragile fractures.

## Conclusion

In this work, weldments made with GMAW using two consumables that have very different levels of tensile strength and ductility were submitted to "in plane" quasi-static and structural impact torsion loads. The results obtained allow the following conclusions:

- For weldments made with AWS ER70S-6, the maximum resisted loads in the quasi-static tests of structural impact are higher than the analytical values.
- For both, the transverse weld beads and "C" configurations, preheating has great influence when using AWS ER 120S-G electrode. It promotes a reduction in the welded joint average hardness and increases its maximum strength for quasi-static and structural impact.
- Areas under the quasi-static loading curves can be related to weldments structural ductility and they have shown also that preheating has a great influence on this mechanical property.
- For both transversal and in "C" configurations, a reduction in the maximum resisted load is observed when the weldments are submitted to structural impact loads, thus showing the need for caution in the dimensioning of welded joints submitted to this loading type.

**Acknowledgment:** To the UFRGS / PROMEC and UFRGS / DEMEC for lending the high-speed camera. To the Physics Teaching Laboratory of the Physics Institute / UFRGS for lending the displacement sensors. To Dr. Gelsa Edith Navarro Hidalgo from the Mineral Processing Laboratory (LAPROM/UFRGS) for assisting in the acquisition of SEM (Scanning electron microscope) images. One of the authors (ADM) thanks to Federal University of Santa Maria (UFSM) for supporting his involvement in this research.

## REFERENCES

Alves, L. M. 2005. Fractal Geometry Concerned with Stable and Dynamic Fracture Mechanics. Journal of Theoretical and Applied Fracture Mechanics, v.44, p.44-57, 2005.

American Institute Of Steel Construction. Welded connections: a primer for engineers. Chicago: AISC, 2006

American Society For Testing And Materials. Astm A36/A36M-14, Standard Specification for Carbon Structural Steel, ASTM International, West Conshohocken, PA, 2014.

American Society For Testing And Materials. Astm E384 – 17, Standard Test Method for Microindentation Hardness of Materials, ASTM International, West Conshohocken, PA, 2017.

American Welding Society. AWS D1.1. Structural welding code: steel. Miami: AWS, 2006.

Beer, P. F.; Johnston, E. R. Vector mechanics for engineers: dynamics. 10th ed. New York: McGraw-Hill, c2013.

Beléndez, A. et. al. Exact solution for the nonlinear pendulum. Revista Brasileira de Ensino de Física, v. 29, n. 4, p. 645-648, (2007).

Blodgett, O. W. Design of Welded Structures. Cleveland. The James F. Lincoln Arc Welding Foundation, 1966.

Broek, D. Elementary Engineering Fracture Mechanics, Martinus Nijhoff Publishers, 3rd revised edition, 1984.

Callister, W. D. Materials science and engineering: an introduction. 8ª ed. Hoboken: John Wiley & Sons, 2009.

Dauskardt, R. H.; Haubensak, F.; Ritchie, R. O. On the interpretation of the fractal character of fracture surfaces. Acta Metall. Mater, v. 38, p. 143-159, 1990.

Dieter, G. E. Mechanical Metallurgy. 2ª ed. Guanabara Koogan: Rio de Janeiro, 1981 (in Portuguese).

Elektriska Svetsnings-Aktiebolaget, ESAB. Consumables quality certificate. Available at: https://www3.esab.com.br/certificado.asp. Accessed in October/2019 (in Portuguese).

European Structural Steel Standard. EN 10025-2: 2004, Grade designations, properties and nearest equivalents.

Image J. National Institutes of Health, USA. https://imagej.nih.gov/ij/.

Jones, N. 2012. Structural Impact. 2a. Ed. Nova York: Cambridge Press.

Johnson, W. *et al*. 1972. Impact strength of materials. Edward Arnold. London.

Kobayashi, T. 2002. Progress in the Instrumented Charpy Impact Test, Materials Science Research International, v.8, n. 3, pp. 141-150.

Machado, I. G. 2011. Design of Fillet Welded Joints: A Critical Review. Soldagem & Inspeção, 16(2): 189-201, Apr/Jun (in Portuguese).

Machado, I. G. 2013. Failures of Welded Steel Structures Due to Reduced Ductility. Soldagem & Inspeção, 18(4): 391-403, Oct/Dez (in Portuguese).

Meyers, M.A. 1994. Dynamic Behaviour of Materials. 2.ed. Wileey-IEEE.

Neal, B. G.1956. The plastic methods of structural analysis. Great Britain: Chapman & Hall.

*******